Available online at www.sciencedirect.com
SCIENCE DIRECT®
Polymer 44 (2003) 5643–5654
polymer
www.elsevier.com/locate/polymer

Toughening high performance ultrahigh molecular weight polyethylene using multiwalled carbon nanotubes

S.L. Ruan[a], P. Gao[b,*], X.G. Yang[b], T.X. Yu[a]

[a]*Department of Mechanical Engineering, The Hong Kong University of Science and Technology, Clear Water Bay, Kowloon, Hong Kong, People's Republic of China*
[b]*Department of Chemical Engineering, The Hong Kong University of Science and Technology, Clear Water Bay, Kowloon, Hong Kong, People's Republic of China*

Received 23 April 2003; received in revised form 29 June 2003; accepted 9 July 2003

Abstract

We report experimental observations on the drastically enhanced toughness in the high-strength and high-modulus ultrahigh molecular weight polyethylene (UHMWPE) films due to the addition of 1 wt% multiwalled carbon nanotubes (MWCNTs). A combination of tensile and Raman spectroscopic measurements showed that the presence of MWCNTs in the composites can lead to a ~150% increase in strain energy density in comparison with the pure UHMWPE film at similar draw ratios. This is accompanied with an increase of ~140% in ductility and up to 25% in tensile strength. We attribute the above observations to the chain mobility enhancement in UHMWPE induced by the MWCNTs.

Keywords: High-strength and High-stiffness UHMWPE films; MWCNT/UHMWPE composite films; Micro-raman spectroscopy

1. Introduction

The unusual electrical and mechanical properties of carbon nanotubes (CNTs) have motivated a flurry of interests to exploit their applications in advanced composite materials, particularly polymer composites, to improve the performance of a matrix or to achieve new properties. It has been reported that CNTs are extremely strong with the strength of tens of GPa and exceptionally stiff with Young's modulus in TPa range, yet remarkably flexible with the break strain larger than 5% [1,2]. In addition, CNTs have high aspect ratios (>100). These properties make it interesting to use CNTs as fillers in ductile nanocomposites. The effective utilization of nanotubes in composite applications depends strongly on the ability to disperse the CNTs homogeneously throughout the matrix without destroying the integrity of the CNTs. Furthermore, a good interfacial bonding is required to achieve load transfer across the CNT–matrix interface, a necessary condition for improving the mechanical properties of polymer composites.

Some experimental studies on CNT-reinforced polymer composites have been reported [3–5]. A 20% increase of modulus in tension and 24% in compression were observed for 5 wt% multiwalled carbon nanotubes (MWCNT)/epoxy composites [3]. Using the surfactant $C_{12}EO_8$ as the processing aid, Gong et al. [4] obtained a 30% increase of elastic modulus with the addition of only 1 wt% CNTs into the epoxy matrix, while the addition of CNTs without the surfactant only has moderate effects on the mechanical properties. For MWCNT/PMMA composites, tensile strength increased 7–30%, toughness ~10% and hardness ~43% with the addition of 1–7 wt% acid-treated MWCNTs [5].

In order to optimize the performance of the CNT reinforced polymer composites, some attempts have also been made to produce alignment of CNTs in the matrix [6–8]. Drawing at temperatures above the glass transition temperatures of the polymer matrix has been shown to be effective to produce uniaxial alignment of CNTs along the draw direction [7]. A most noticeable enhancement in tensile stiffness has been reported. However, the alignment caused a significant loss of ductility. Such observations also led to speculations that the effect of CNTs on polymer composites may be similar to that of nano-carbon fiber.

* Corresponding author. Tel.: +85-223587126; fax: +85-223580054.
E-mail address: kepgao@ust.hk (P. Gao).

0032-3861/$ - see front matter © 2003 Elsevier Ltd. All rights reserved.
doi:10.1016/S0032-3861(03)00628-1

Hence, the resilience of CNTs does not have any effects on the composites.

In this paper, we report the effect of MWCNTs on mechanical properties of highly anisotropic ultrahigh molecular weight polyethylene (UHMWPE) films prepared by intimately mixing 1 wt% CNTs with UHMWPE followed by solution casting and hot draw. We believe this is the first report that shows the incorporation of CNTs into UHMWPE matrix enhances the ductility significantly as well as the strain energy absorption before fracture.

2. Experimental

2.1. Preparation of MWCNT/UHMWPE composite

The composites used in the present study were made of UHMWPE HiFax 1900 reactor powders with molecular weight of 6×10^6 g mol^{-1} kindly supplied by Basell Ltd, USA, and MWCNTs with diameters of the order 15 nm. The as-received MWCNTs were in the form of clusters under scanning electron microscopy (SEM). All CNTs were purified by following the treatment procedures developed by Windle et al. [9] before use. The purified CNTs were dispersed in xylene by magnetic stirring for 2 h followed by a 2 h of ultrasonic vibration at the ambient temperature. The CNT–xylene mixture was poured into the UHMWPE–xylene solution refluxed at 140 °C for 3 h and the whole mixture was further refluxed for 30 min in order to disperse the CNTs into the UHMWPE solution. The precursory 1 wt% MWCNT/UHMWPE films were prepared by solution casting. The pure UHMWPE films were also prepared in a similar manner. The final anisotropic films with different hot-drawn ratios were obtained by tensile draw at 120 °C using an Instron tensile tester (Model 5567). The draw ratio was determined by measuring the cross-sectional area ratios directly. Whilst the width can be readily measured using a micrometer, the film thickness had to be measured by a Surface Profile System (alpha-step 200) since the drawn films are very thin, of the order of a few μm.

2.2. Tensile test

Mechanical properties of the drawn films were measured by the Instron tensile test (load cells 10 and 100 N) and a MiniMat 2000 (load cell 20 and 100 N). All tests were conducted at the ambient temperature using a cross-head speed of 2.5 mm min^{-1}. The specimens were prepared by gluing the films on paper board frames with suitable dimensions. The gauge length was 10 mm.

2.3. Micro-Raman spectroscopy

The Raman Spectra for both MWCNT/UHMWPE composites and pure UHMWPE films were obtained using a Renishaw micro-Raman system 1000 in conjunction with a specially made load cell as well as the MiniMat 2000. The excitation source was an argon laser with the wavelength of 514.5 nm and the spectra data were collected in the 180° backscattering mode. The laser beam was 25% de-focused together with a 50x objective lens to produce a 20–30 μm diameter laser spot to minimize laser beam heating effects as well as to have a larger sampling volume. To minimize stress relaxation as well as heating effects, 5 scans were used for each spectrum collection. All selected bands were fitted and deconvoluted when necessary using a combination of Gaussian and Lorentzian functions.

3. Results and discussion

3.1. Morphology of MWCNTs and composite films

The as-received MWCNTs were observed in the form of clusters and had many impurities by SEM as shown in Fig. 1(a). After the acid-treatment, the content of CNTs was increased and the typical rope status of CNTs can be readily seen (Fig. 1(b)). High resolution TEM photos show that these CNTs are of diameters ~15 nm, Fig. 1(c).

The morphology of the 1 wt% UHMWPE/MWCNT composite film is shown in Fig. 2. Several interesting observations can be made from these micrographs. First, the MWCNTs appear to disperse in the form of 1 μm diameter clusters. These clusters appear to be the center for PE crystal growth. Secondly, a magnified view of the clustered region shows that the CNTs are fully dispersed as individual nanotubes, although, some are entangled together in the form of random arrays. No ropelike regions are observed, implying that the solution mixing was effective in separating the CNTs.

The morphology of the drawn films is observed by a combination of optical microscopy (OM), SEM and atomic force microscopy (AFM). For all observations made here the 1 wt% MWCNT/UHMWPE film was drawn to a draw ratio of ~30. Clearly, a uniform distribution of CNTs in the highly drawn PE matrix can be observed under OM. The OM was performed by heating the film under constraint until 150 °C to minimize the interference of the aligned PE fibers with the phase contrast between PE and CNT, Fig. 3(a). Micro-Raman spectra using 1 μm spot size taken at a range of positions also confirm that the CNT distribution is uniform at least at the micrometer scale. The AFM micrograph shown in Fig. 3(b) shares a similar feature to the OM observation and shows that the CNTs are apparently clustered together to form 30 to 90 nm clusters. The most striking feature shown in Fig. 3(b) is the apparent transverse bridges between the highly aligned fibers. These transverse bridges are of similar diameters of ~30 nm and are uniformly dispersed throughout the sample area. This feature is however, absent from the pure PE sample at a similar draw ratio, Fig. 3(c). Scanning electron microscopic examination on the composite film shows that these

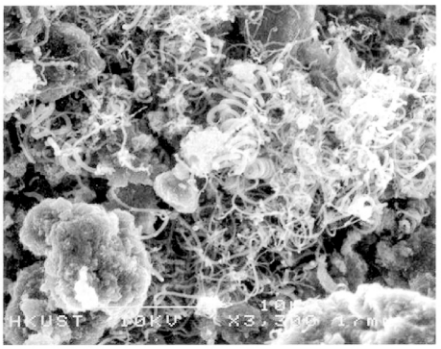

(a)

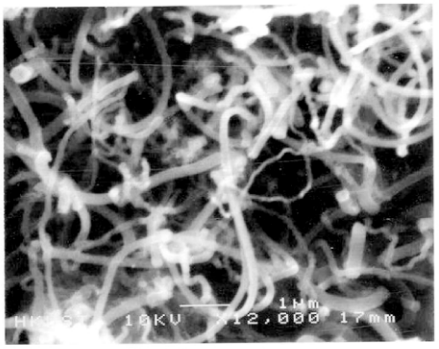

(b)

(c)

Fig. 1. Morphology of the multiwalled carbon nanotubes (MWCNTs) used in this study observed by SEM and TEM. (a) The as received MWCNTs showing the presence of amorphous carbons; (b) The purified MWCNTs show an increased CNT content with amorphous carbons removed; and (c) high resolution TEM photo showing that the MWCNTs are capped with diameters ~15 nm.

transverse fibers are most likely the macro-shish-kebab crystals [10], Fig. 3(d). Of course, the resolution of the SEM is limited the sizes observed are different. It is worth-well to mention here that the CNT/PE composite film is visually much smoother than the drawn PE films at similar draw

(a)

(b)

Fig. 2. Morphology of the un-drawn 1 wt% MWCNT/UHMWPE films observed using TEM. (a) A global view showing the macroscopic distribution of the embedded CNTs and their effects on PE crystallization. No staining was applied but the PE phase displays a clear lamellar structure radiating from the clustered CNTs. (b) A magnified view of one of the clustered CNT regions displaying the dispersion of CNTs as individual tubes. Some clusters on the nano-scale show local entanglements between CNTs.

ratios. Fibrillation is absent in all MWCNT/UHMWPE films but readily occurs in the drawn PE films at draw ratios above 20.

3.2. Mechanical properties

First, we examined the effect of MWCNTs on the

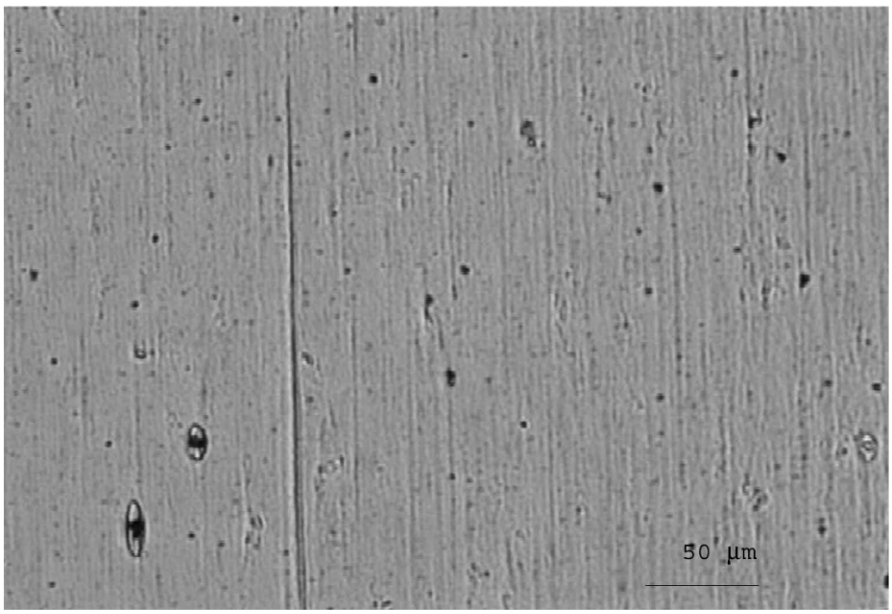

(a)

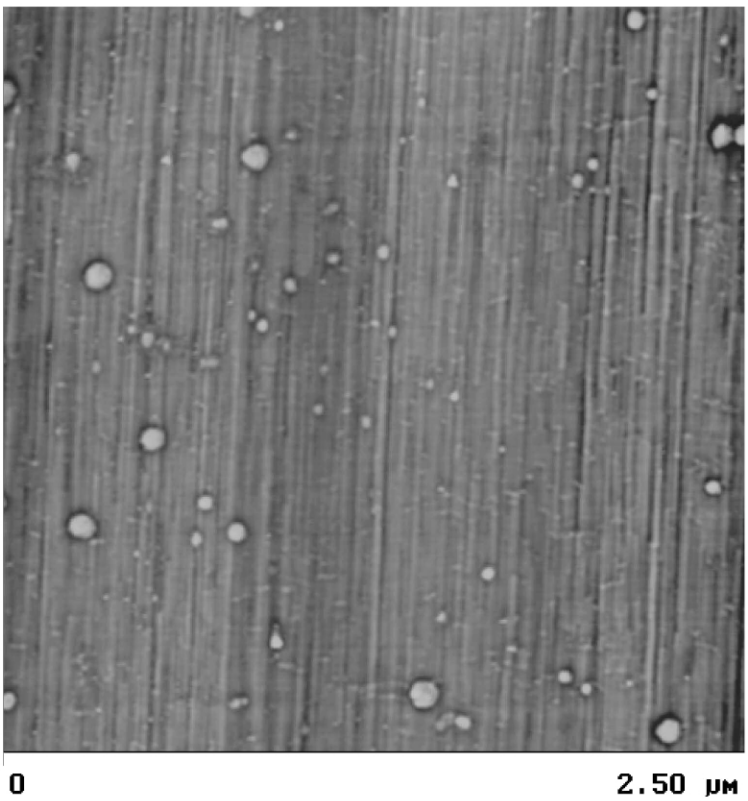

(b)

Fig. 3. Morphology of the 1 wt% MWCNT/UHMWPE composite films at an initial draw ratio of ~30. (a) OM micrograph displaying the microscopic dispersion of CNTs in the drawn film. The photo was taken at 150 °C by constrained heating of the film from room temperature. (b) AFM micrograph of the composite film showing that the CNTs are clustered to form mainly 30–90 nm diameter clusters. Alignment of CNTs cannot be reviewed. (c) The AFM micrograph of pure UHMWPE film at a draw ratio of 30 taken at similar conditions to that in 3(b). and (d) SEM micrograph of the 1 wt% MWCNT/UHMWPE film displaying a clear shish-kebab crystal morphology.

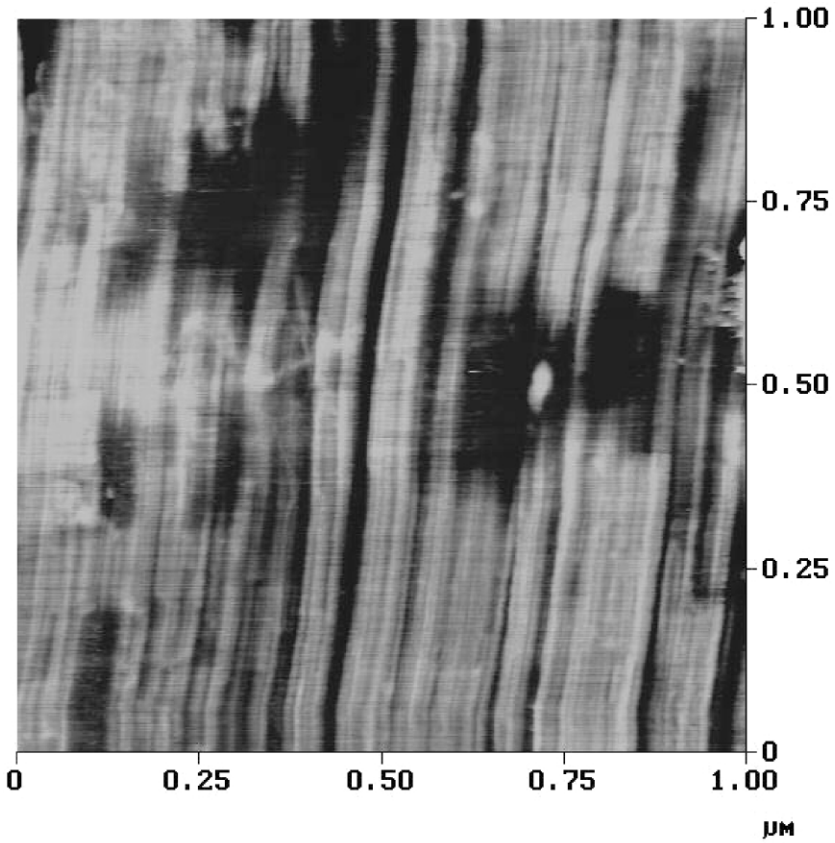

(c)

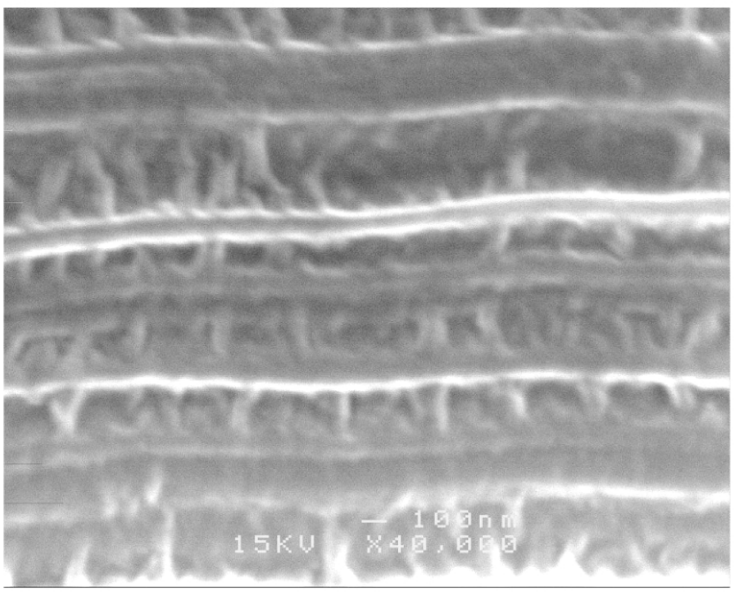

(d)

Fig. 3 (*continued*)

Table 1
Mechanical properties of composites and corresponding pure UHMWPE films

Sample	Young's modulus, E (MPa)	Yielding stress, σ_y (MPa)
1 wt% MWCNT/UHMWPE	1352.3 ± 40.7	12.38 ± 0.84
UHMWPE	977.4 ± 16.2	8.27 ± 0.25

mechanical properties of composite films without hot draw. The films were cut into pieces with the width of 4 mm. The thickness directly measured by micrometer was in the order of tens of μm. From the results as shown in Table 1, a 25% increase in Young's modulus and 47.6% increase in yielding stress were observed. The strain at break was larger than 100% for all samples.

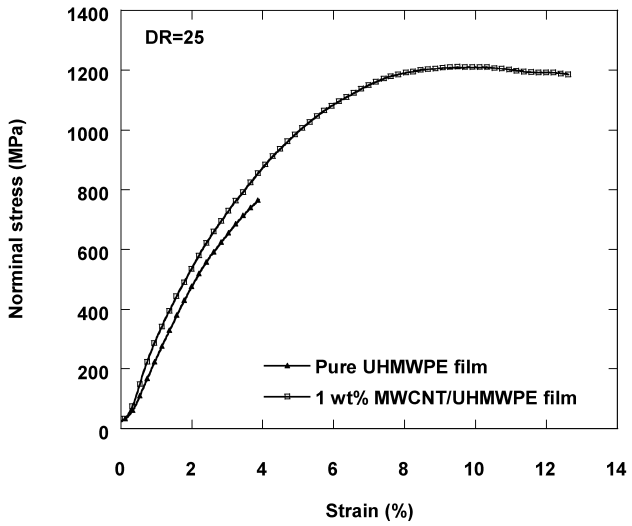

(a) DR≈25

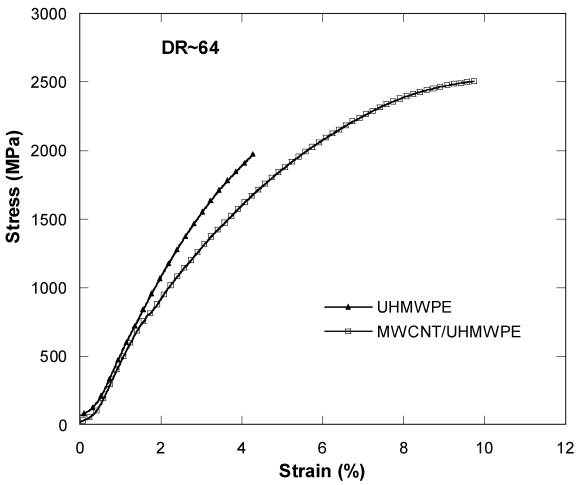

(b) DR≈64

Fig. 4. Real-time stress–strain curves for the drawn films with two different draw ratios at a stretching rate of 2.5 mm min^{-1} and at the ambient temperature.

Secondly, the anisotropic films were drawn from these precursor films at 120 °C to a range of draw ratios. One of the most interesting observations here is the exceptionally high ductility in the composite film. In order to illustrate this, real time stress–strain curves of CNT composites and pure PE films are plotted in Fig. 4 at two different draw ratios. The pure PE films show a near Hookean tensile behavior and the maximum strain at fracture is almost independent of draw ratios. These are in agreement that of the gel spun fibers as observed before [11]. On the other hand, the 1 wt% CNT/PE composite film shows a ductile stress–strain response and the maximum strain at break decreases with increasing draw ratios.

Fig. 5 summarizes the effect of draw ratio on the tensile modulus and tensile strength for the 1 wt% MWCNT/

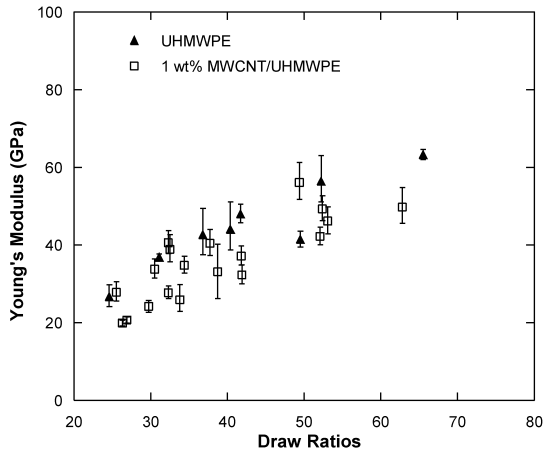

(a)

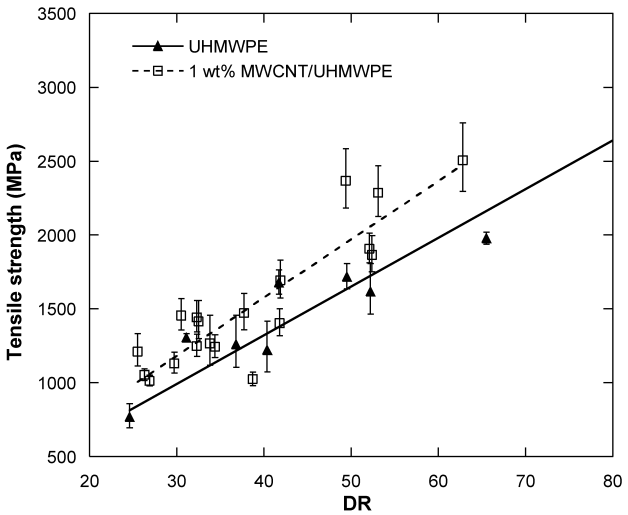

(b)

Fig. 5. Effect of draw ratio on the tensile modulus (a) and tensile strength (b) of the 1 wt% MWCNT/UHMWPE and pure UHMWPE films obtained from the stress–strain curves as shown in Fig. 4.

UHMWPE composite films. The data on the pure UHMWPE films are also presented for comparison. Apparently, the composite films and the pure UHMWPE share similar tensile moduli at all draw ratios, Fig. 5(a). In fact, the pure UHMWPE films appear to show a slightly larger modulus at similar draw ratios. This may be surprising at first sight since there is significant improvement of tensile stiffness even without any draw. However, this may also be expected result given the fact that no apparent alignment of CNTs along the draw direction was observed. Experiments on anisotropic fibers prepared from single walled CNTs show that a maximum tensile strength of 15 GPa [12]. This value is significantly lower than the theoretical estimate of single CNT fibers. As all films have moduli in excess of 20 GPa, the CNTs may not impart additional moduli enhancement if they are not fully aligned along the draw direction and each act as individual tube with no defects. The apparent entanglement between individual tubes and the inevitable curvature observed prior to draw in Fig. 2(b) imply that these embedded MWCNTs are to the best of moduli similar to the anisotropic pure fibers.

The tensile strength of the composite is, however, apparently much higher than the pure PE films at all draw ratios, Fig. 5(b). There is also a tendency for the enhancement in tensile strength due to CNT inclusion to increase with increasing draw ratios. A conservative estimate based on linear fitting to both fibers gives an increase of 25% with 1 wt% MWCNT loading. The true tensile strengths of the composite fibers are higher since the tensile strains at fracture are significantly larger for the composite films and the values used here are nominal stresses.

The enhancement in tensile strength is most likely due to the analogous effects of CNTs to that of the 'taut-tie' molecules in UHMWPE at high draw ratios [13]. The taut-tie molecules have been shown to act as the load bearing centre in the gel spun fibers. The entangled CNTs are unlikely to be pulled apart at high temperatures during tensile draw and they may form knots and hence show a similar role to the taut tie molecules.

The maximum strain at break and strain energy density are the two most affected properties with the introduction of 1 wt% MWCNT. Fig. 6(a) shows the maximum strain at break versus draw ratio. For the pure UHMWPE, the maximum strain at break shows little dependence on draw ratios and all films break at about 5% strain. On the other hand, the composite films show a larger variation ranging from 8 to 12% with a possible trend of decreasing maximum strain at break with increasing draw ratios. These values are, however, 60–140% larger than the pure UHMWPE films, implying that the presence of CNT significantly improved the ductility of the composite films.

The toughness (or strain energy density) versus draw ratio obtained by integration of the area under the stress–strain curves for both pure and composite films containing 1 wt% MWCNT is shown in Fig. 6(b). Whilst both films

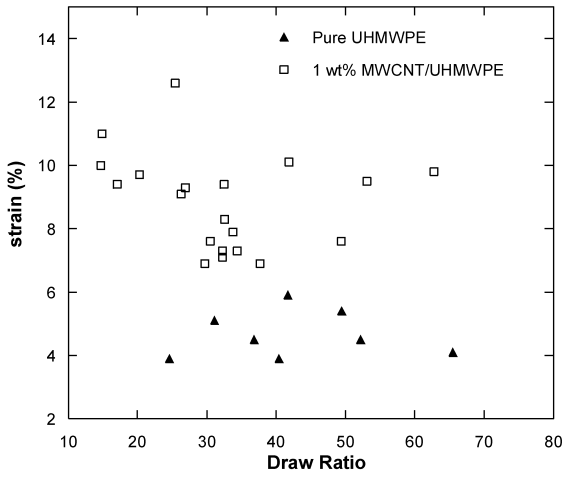

(a)

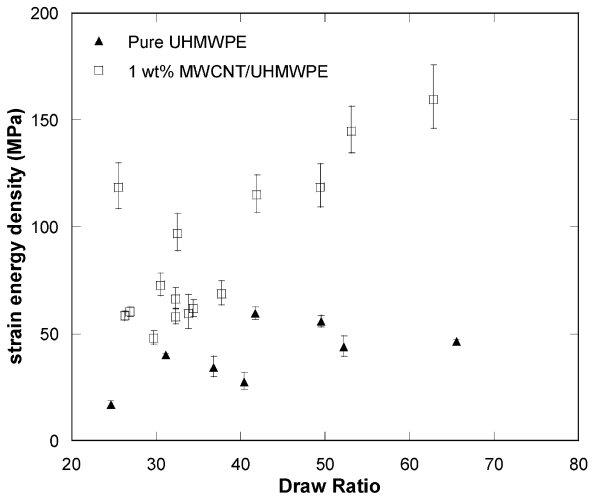

(b)

Fig. 6. Effect of draw ratio on (a) the ductility and (b) the toughness (or strain energy density) of the 1 wt% MWCNT/UHMWPE and pure UHMWPE films. The ductility was obtained directly from the stress–strain curves as shown in Fig. 4. The strain energy density was obtained by integrating the areas under these stress–strain curves.

show increase of toughness with draw ratios, the composite films show a much steeper increase. The maximum toughness of the composite fiber is 150 MPa but the pure PE film at the same draw ratio is only about 60 MPa. This represents an enhancement of up to 150%.

These unexpected enhancements in ductility and toughness deserve further discussion. As the CNTs have not shown to produce any stiffness enhancement, the increased ductility is then most likely due to the chain mobility enhancement in the presence of CNTs. The mechanical-Raman study to be shown below also supports this proposition. The nano-scale dispersion of CNTs in the composite film and good interfacial bonding with the neighboring PEs enable the CNTs to act as nucleating

centers for PE crystal growth. The TEM micrograph in Fig. 2(a) shows clearly the CNTs are the nucleating centre for the lamellar growth of PE crystals. These secondary crystals may also grow during hot draw at 120 °C. The AFM and the SEM micrographs (Fig. 3(b) and (d)) have demonstrated the presence of the shish-kebab crystals in the composite films that are not seen in the pure PE films. Apparently, such secondary crystals are much more mobile than the all extended PE crystals and hence lead to a significantly enhanced ductility in the composite films. The interface load-transfer analysis using mechanical-Raman spectroscopy to be presented below also supports this argument.

Experiments on CNT reinforced polymer composite have so far shown that intimate bonding and load transfer is the key for mechanical property enhancement. Mechanical-Raman spectroscopy has been the most effective means for characterizing the molecular deformation mechanism as well interfacial load transfer. This is presented in Section 3.3.

3.3. Load transfer

The effective techniques used to understand the load transfer and failure of nanotubes are micro-Raman spectroscopy [14,16] and a Kelly–Tyson approach to measure the interfacial shear stress [15]. The second-order A_{1g} (disorder-induced) Raman band is usually used to monitor the deformation of CNTs in the polymer matrix due to the large peak shift within applied composite strain if the nanotubes are carrying strain. Lourier and co-workers [16] have observed 6 cm^{-1} in MWCNTs under hydrostatic compression using thermal loading and even larger shifts for SWCNT samples. Schadler et al. [14] observed a similar shift in MWCNTs in compression and no shift in tension. These techniques have given some evidences for good load transfer between the polymer and the nanotubes. The Raman spectra of as-received and acid-treated 15 nm-diameter MWCNT powder using a 514.5 nm Argon laser are shown in Fig. 7(a). It can be seen from the spectra that the acid-treated MWCNTs show three well-defined Raman bands at 1348, 1574 (with another weak peak 1612 cm^{-1} by band deconvolution), and 2691 cm^{-1}, which are termed the D-band, G-band and D*-band (or G'-band [17], overtone of D-band), respectively [18]. The as-received MWCNT peak positions are indicated in brackets. The spectrum of MWCNTs resembles closely that of carbon fibres and graphite. It has been reported that a graphite single crystal induces a single Raman band at 1600 cm^{-1} (E_{2g} mode), while polycrystalline graphite gives rise to an additional band at about 1350 cm^{-1} (A_{1g} mode) [19]. Obviously, the present bands at 1348 and 1577 cm^{-1} correspond to A_{1g} and E_{2g} mode, respectively. The acid treatment significantly enhanced the peak intensity at 1350 cm^{-1} and in the meantime, produced a blue shift of all peaks. This may suggest that the CNTs are packed closer after the removal of amorphous carbons.

Compared to the Raman spectrum of the purified MWCNTs, the incorporation into UHMWPE matrix resulted in a further blue peak shift, which means the MWCNT is subjected to a compressive stress [20]. This can be attributed to the contraction of PE matrix during cooling. This is shown in Fig. 7(b). It should also be noted that there are spectra overlaps at 1350 and 2700 cm^{-1} between the undrawn PE and the MWCNT. However, at high draw ratios, the band at 2700 cm^{-1} for PE disappears (Fig. 7(c)), and hence can be used for the analysis of the mechanical-Raman response of the embedded MWCNT.

The Raman spectrum of pure PE has been widely studied, and a comprehensive review on the vibrational behavior of PE is available [11,21], with the major features of the crystalline spectrum unambiguously assigned. Both the C–C asymmetric stretching mode B_{1g} (1060 cm^{-1}) and symmetric stretching mode A_{1g} (1130 cm^{-1}) bands have been observed to shift to lower wave numbers under tension in the highly oriented PE fibers. Some authors have reported the band split of these peaks either under or without any stresses. It was generally accepted that the peak shift of the 1060 cm^{-1} band is appropriate to describe the molecular level deformation behavior of high-modulus and high-strength polyethylene fibers. The 1130 cm^{-1} band may potentially overlap with the 1060 cm^{-1} band especially during tension loading, and does not shift so much in comparison, and thus is not used as frequent. In this study, we have investigated the peak shift of both bands and found that they show similar level of shift with strain for both the pure UHMWPE fiber and the 1 wt% MWCNT/UHMWPE composite fiber. Therefore, the peak-shifts of both bands versus strain are presented.

The samples for mechanical-Raman testing are of draw ratios 29 for the pure UHMWPE film (Young's modulus ~30 GPa, tensile strength ~1.0 GPa) and 33 for the 1 wt% MWCNT/UHMWPE film (Young's modulus ~31 GPa, tensile strength ~1.3 GPa).

Before the overall spectra shift results are presented, the band shape and peak-shifts at a few selected strains are presented in Fig. 8 to show the way how peak shifts are obtained at different strains for both the PE chains as well as the embedded MWCNTs. All bands were fitted using a combination of Gaussian and Lorentzian functions. An example is shown in Fig. 8(a) where both the original spectra and the fitted spectra are shown in the graph.

Fig. 9 shows the peak-shift of the D*-band of the MWCNTs versus strain for the 1 wt% MWCNT in UHMWPE during tension. The peak positions show a great deal of scatter, especially at strains between 1 and 10%. A detailed examination of the spectra shift can lead to the classification of the deformation behavior into four regimes: (i) in the first 1% of strain, a clear red-shift is observed. The spectra shift is approximately linear. (ii) When the strain is between 1 and 10%, a significant red–blue shift is observed. (iii) At strains between 10 and 15%, the spectra shifts show a reduced scatter but a clear red shift

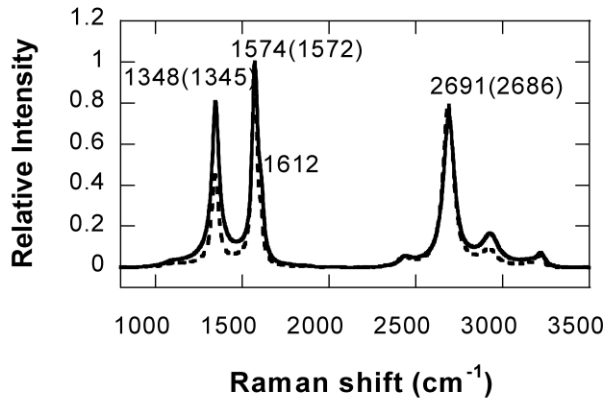

(a)

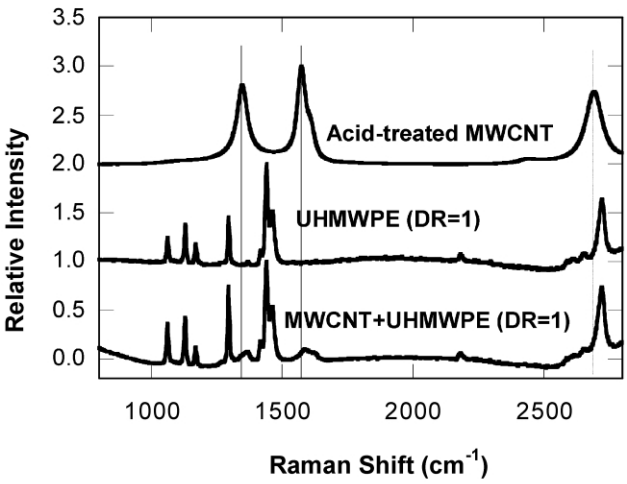

(b)

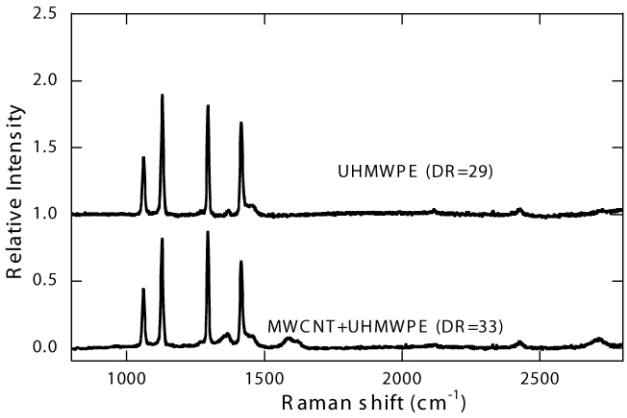

(c)

Fig. 7. Overall Raman spectra displaying the characteristic features of the materials used in this study measured at room temperature using Argon laser with the wavelength of 514.5 nm at 20 mW. (a) Pure MWCNTs with and without purification:- - - as received MWCNTs; and — acid-treated MWCNTs. (b) Purified MWCNTs and the undrawn pure UHMWPE and the undrawn 1 wt% MWCNT/UHMWPE film. Three light vertical lines were drawn through the peak positions of the three characteristic bands for MWCNT at 1350, 1600, and 2700 cm^{-1} wavenumbers, respectively. (c) The anisotropic 1 wt% MWCNT/UHMWPE and pure UHMWPE films with draw ratios ~30.

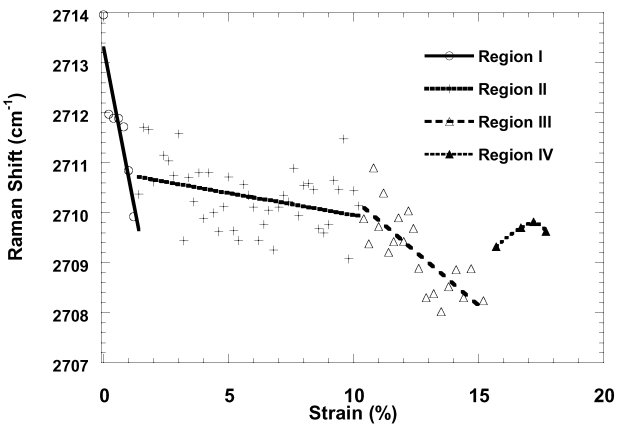

Fig. 9. Variation of the CNT D*-band versus tensile strain within the 1 wt% MWCNT/UHMWPE composite films obtained from spectra shown in Fig. 8. Region I: elastic region; Region II: viscoelastic and plastic deformation occurs; Region III: strain hardening occurs; and Region IV: partial failure at the microscopic level takes place in the matrix. Linear least square fits were applied for regions I-III. For region IV, interpolation of data points was made to display the trend.

again. (iv) At strains above 15%, blue shift is observed, showing that the MWCNTs are experiencing compression. Overall, the total red shift is 6 cm^{-1} and this is perhaps the largest red-shift in polymer nanotube composites reported to date.

The red-shift observed at low and high strains (regions (i) and (iii)) suggest that the MWCNTs embedded inside the composite fiber are experiencing tensional loading, an intimate load transfer through the PE-MWCNT interface may be envisaged. The oscillatory response at the intermediate strains (region (ii)), however, may suggest that there is a stick and slip at the interface. This could happen if the matrix is yielding. In fact, this proposition is consistent with the spectra shift in the matrix PE to be shown below. At the very high strain range, above 15% (region (iv)), the compressive response shown here may be due to the local microscopic failure within the matrix. Once the matrix buckles, a large compressive stress will be transferred to the MWCNTs.

The spectra shifts for the bands at 1060 and 1130 cm^{-1} for UHMWPE with and without the 1 wt% MWCNT are shown in Fig. 10.

Clearly, the spectra shifts for both the 1060 and 1130 cm^{-1} bands are similar. The discussion below will focus on the 1060 cm^{-1} band, as it has a slightly larger shift than the 1130 cm^{-1}. It can be seen that there exist clear differences between the spectra shifts for the pure UHMWPE and UHMWPE containing 1 wt% MWCNT. The pure UHMWPE shows essentially a two-zone response, with a large (~5 wavenumbers) and quasi-linear response for strains up to 5% followed by a nearly constant peak shift at larger strains. The pure film breaks at about 10% strain and a compressive response is observed before failure. These results are consistent with other literature reported responses in high performance UHMWPE fibers [21].

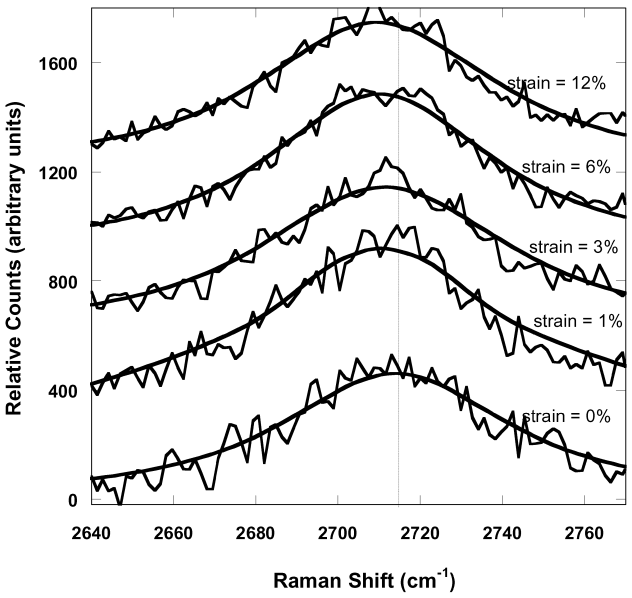

(a)

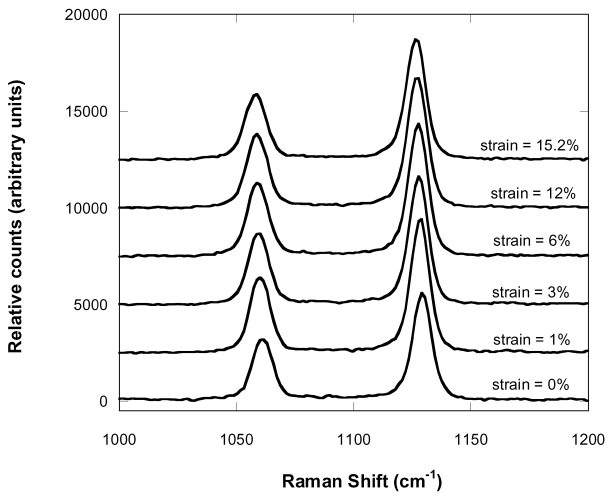

(b)

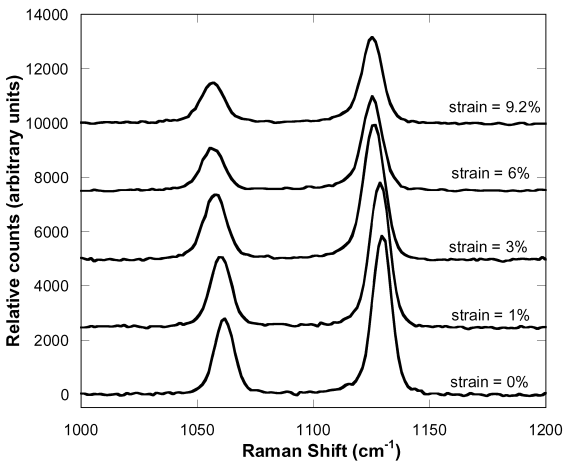

(c)

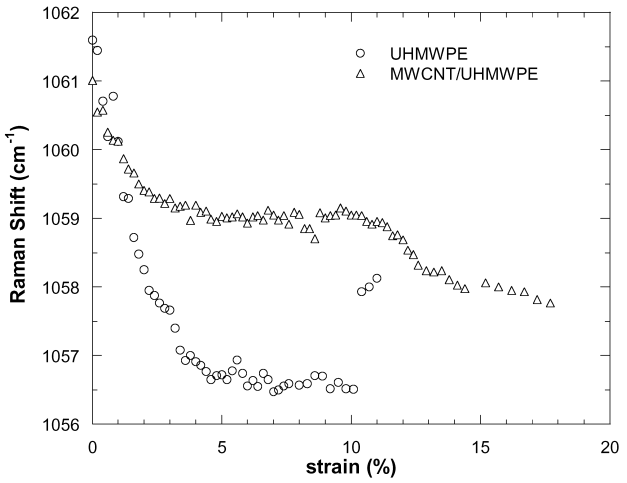

(a)

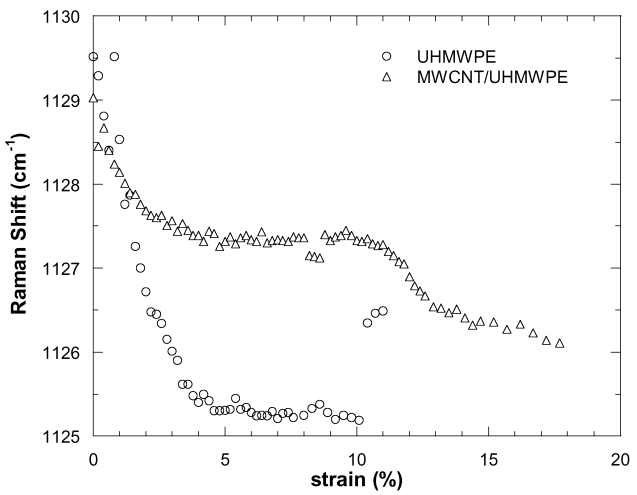

(b)

Fig. 10. Variation of the asymmetric and symmetric C–C band shift for PE chains with and without the incorporation of the 1 wt% MWCNTs against different tensile strains obtained from spectra shown in Fig. 8.

Fig. 8. Selected bands displaying spectra shifts versus applied strains. (a) Raman shift of the D*-band for the embedded MWCNTs in the 1 wt% MWCNT/UHMWPE film at different strains. The continuous thick and solid lines are the fitted spectra using a combination of Gaussian and Lorentzian functions. The vertical line was drawn through the peak of the band prior to tensile strain. (b) Raman shift of the asymmetric C–C stretching B_{1g} and symmetric C–C stretching A_{1g} bands for the PE chains in the 1 wt% MWCNT/UHMWPE films at different tensile strains. (c) Raman shift of the asymmetric C–C stretching B_{1g} and symmetric C–C stretching A_{1g} bands for the PE chains in the pure UHMWPE films at different tensile strains.

On the other hand, the C–C stretching peak for the UHMWPE containing 1 wt% MWCNT shows a very different response with increasing strains. First, it may be seen that at strains less than 2%, a quasi-linear response may also be observed followed by a very small further red-shift to strains up to 5% and near constant peak shift for strains up to 10%. Further increase in strain causes a second stage of red-shift similar to what is shown by the embedded MWCNT (region (iii) in Fig. 9). At the very high strains, above 15%, a second near plateau region (slight further red-shift) is shown. Overall, the spectra shift for the UHMWPE in the composite film is smaller than that in the pure UHMWPE (~3 wavenumbers for the whole deformation range).

These observations suggest the presence of MWCNT enhances the chain mobility of UHMWPE. In the true elastic limit (strains $<1\%$), the C–C stretching of PE chains is not affected by MWCNT. This may explain why the initial tensile modulus of the composite fiber is similar to that of the pure UHMWPE film at similar draw ratios. Although, the MWCNT is experiencing tension in this range, its curved shape plus entangled arrangement (Fig. 2(b)) may not impart a significant effect on the stiffness of the matrix. In fact, it has been shown that anisotropic fibers prepared from single walled CNTs only show modulus up to 15 GPa. This is significantly lower than the theoretical estimate [12]. The PE films here possess moduli in excess of 20 GPa, and hence it is unlikely, significant enhancement in the modulus of the composite fiber can be achieved unless all CNTs are made to align individually with each tube bonded to the PE matrix. The earlier than expected deviation from linear elastic response in the composite fiber (~2% strain) is most likely caused by the deformation of the secondary shish-kebab crystals whose population was large due to the nucleation effects of the embedded CNTs (Fig. 3). This feature is absent from the pure UHMWPE film. The secondary crystals formed due to the MWCNTs (Figs. 2(a) and 3(d)) are of higher mobility. At very high strains (10–15%), the mobility of all PE chains becomes reduced again and strain hardening effect sets in, and hence a further red-shift is observed. The strain hardening effect observed at large strains in polyethylene chain may be due to the load-bearing effects imparted by the embedded CNTs. The CNTs apparently are curved, Fig. 2(b), and show some degree of entanglement. These maybe hard to become extended during hot draw and hence will eventually become the knots within the composite films. The MWCNT knots will then also limit the further stretching of the PE chain. As alluded above, these knots become the load bearing centre at very large strains similar to the taut-tie molecules in PE [13]. These knots are also the centre where the concentration of secondary crystals is higher and hence impart a higher ductility at the intermediate strains. The different responses at strains above 15% for the PE chain and the MWCNTs may be because the failure is microscopic. For the PE phase, majority of the chains are still intact and being further stretched, so the overall response is still tension. On the other hand, the MWCNT is the in minor phase and the centre for load bearing, failures of the PE chains in the immediate vicinity will lead to a compressive loading to the embedded MWCNTs.

These mechanical-Raman results are consistent with the tensile test data and both show that the composite films show much higher ductility. In the meantime, it should also be noted that the strain range in the micro-Raman spectroscopy is larger than that in tensile test. Although, every care is taken to ensure the stress-relaxation after each strain is minimized by taking very few scans plus large spot sizes by defocusing the beam, this behavior will still dominate at large strains. The data, however, are not affected at small strains as illustrated by the real time stress–strain–time curves. The absence of apparent strain-hardening in the nominal stress–strain curves (Fig. 4) illustrates the differences between the macroscopic mechanical measurement and the microscopic deformation behavior. Of course, the true stresses continuously increase with strain after yielding (Fig. 4(a)), and hence the large strain response observed in the mechanical-Raman experiments may manifest this increase at large strains.

4. Conclusions

In summary, the incorporation of 1 wt% MWCNT reinforcement produces a remarkable increase in the tensile strength and modulus for non-drawn UHMWPE composite films of 49.7 and 38%. For the anisotropic MWCNT/UHMWPE composite films with high draw ratios, an up to 150% increase in strain energy density has been observed together with a simultaneous increase of tensile strength of ~25% and an increase of ductility up to 140%. The tensile modulus of the composite film appears to be little effected. This is, however, expected because of the possible low tensile modulus of the incorporated MWCNT [6].

A good load transfer at the PE/MWCNT interface has also been observed in the micro-Raman mechanical spectroscopy. The large ductility increase in PE has been attributed to the secondary crystal formation due to the presence of MWCNTs. The increase in the ultimate tensile strength of the composite fiber is attributed to the load bearing effect by the embedded CNTs similar to the taut-tie molecules in polyethylene [14]. These structures may have potential applications in limiting the ultimate creep responses of the high performance UHMWPE films. High-strength and high-modulus UHMWPE fibers have been commercialized for about two decades after the discovery of gel-spinning process by Smith et al. [22], one of the major problems limiting their application has been the low creep resistance. Slippage between fibers has been the main cause for the low creep resistance. If the incorporation of CNTs can lead to an increase of knots concentration in the spun

fiber, the natural bio-compatibility and low frictional resistance of CNTs may broaden its application for the composite fiber in the biomaterials area.

Acknowledgement

This project was funded by the Research Grant Council of Hong Kong with an earmarked grant for research, grant no. HKUST 6244100P.

References

[1] Baughman RH, Zakhidov AA, de Heer WA. Science 2002;297:787.
[2] Yu MF, et al. Science 2000;287:637.
[3] Schadler LS, Giannaris SC, Ajayan PM. Appl Phys Lett 1998;73(26):3842.
[4] Gong X, et al. Chem Mater 2000;12:1049.
[5] Jia Z, et al. Mater Sci Engng A 1999;271:395.
[6] Ajayan P, Stephan O, Colliex C, Trauth D. Science 2000;287:637.
[7] Jin L, Bower C, Zhou O. Appl Phys Lett 1998;73:1197.
[8] Bower C, Rosen R, Lin J, Han J, Zhou O. Appl Phys Lett 1999;74:3317.
[9] Shaffer MSP, Windle AH. Adv Mater 1999;11:937.
[10] Huong DM, Drechsler M, Möller M, Cantow HJ. J Microsc 1992;166:317–28.
[11] Tarantili PA, Andreopoulos AG, Galiotis C. Macromolecules 1998;31:6964–76.
[12] Vigolo B, Pénicaud A, Coulson C, Sauder C, Pailler R, Journet C, Bernier P, Poulin P. Science 2000;290:1331–4.
[13] Prasad KV, Grubb DT. J Polym Sci, Part B: Polym Phys 1989;27:381–403.
[14] Schadler LS, Giannaris C, Ajayan PM. Appl Phys Lett 2000;12:750.
[15] Wagner HD, Lourie O, Feldman Y, Tenne R. Appl Phys Lett 1998;72:188.
[16] Lourie O, Wagner HD. J Mater Res 1998;13:2418.
[17] Cooper CA, Young RJ, Halsall M. Compos: Part A 2001;32:401.
[18] Yuang Y, Young RJ. J Mater Sci 1994;29:4027.
[19] Tuinstra E, Koening JI. J Chem Phys 1970;53:1126.
[20] Siesler HW, Infrared and Raman spectroscopy of polymers, Marcel Dekker, Inc; 1980.
[21] Gall MJ, Hendra PJ, Peacock CJ, Cudby MEA, Wills H. Spectrochim. Acta, Part A 1972;28:1485–96.
[22] Smith P, Lemstra PJ. J Mater Sci 1980;15:505–14.